WBAN Off-Body Channel Angular Structure Comparison between SAGE Estimation and Ray Tracing Simulation

Nicolas Amiot, Meriem Mhedhbi, Bernard Uguen, Raffaele Derrico

WBAN Off-Body Channel Angular Structure Comparison between SAGE Estimation and Ray Tracing Simulation

Nicolas Amiot[#], Meriem Mhedhbi[#], Bernard Uguen[#], Raffaele DErrico[†]

[#]University of Rennes 1, IETR, CNRS UMR6164, Rennes, France
[†]CEA, LETI, MINATEC Campus, Grenoble, France
Email: {nicolas.amiot, meriem.mhedhbi, bernard.uguen}@univ-rennes1.fr, raffaele.derrico@cea.fr

***Abstract*—In this paper, we present a comparison between Off-Body channel characteristics estimated with Space-Alternating Generalized Expectation-Maximization (SAGE) algorithm from measurement data and those obtained from ray-tracing simulated data. Measurement data were obtained considering a body-worn antenna on a phantom and an external one simulating an access point. The chosen simulation approach takes into account the influence of the body directly into the antenna radiation pattern, and not by including a dedicated body representation into the simulated environment. This simplified approach provides a good agreement between simulation and measurement in terms of received power and Angle of Arrival retrieval.**

***Index Terms*—Body Area Networks, Ray tracing, Channel model, Multipath Channels, Path Loss, Direction-of-Arrival, SAGE**

I. Introduction

Considering both the emergence of wearable devices (smart watches, connected glasses) carried by the quantified-self trend, and Ultra Low Power radio technologies capabilities enabled by e.g. the Ultra Wideband (UWB), Wireless Body Area Networks (WBAN) could be massively disseminated in the public space in the near future.

Regarding the limited available energy and interoperability requirements of those devices, a good understanding of channel characteristics has a fundamental importance in order to design operative and reliable communication systems [1][2]. Indeed, Physical layer (PHY), Medium Access Control (MAC) and Upper Layers protocols performances are strictly dependent to the knowledge of propagation mechanisms and channel models. Consequently, different WBAN channels depending on the wireless node position have to be defined [3].

In the particular case of the Off-Body channel, one of the end points of the link designates a device placed on a human body and the other, far from it, is an external fixed device e.g. a gateway or a router [4].

A deterministic description of the Off-Body channel should consider diffraction and/or shadowing effect of the body(ies) parts, in addition to the classical propagation phenomena. The use of a ray-tracing (RT) tool can be considered in the specific context of WBAN for predicting the Off-Body channel, allowing the future design of communication and localization systems.

Such a simulator has to accurately take into account both the movement of the body and the associated on-body antennas positions, orientations and perturbed radiation pattern. Indeed, one of the specific aspect of the WBAN channel is the dependency of antenna characteristics on the body [5] [6] [7], where the proximity of a human body affects the antenna radiation pattern and thus the channel observation. Then, it is mandatory to properly describe the antenna at both ends of the radio link to correctly predict the channel in terms of power and angles of arrivals (AoA).

The open source mobility-oriented ray-tracing tool PyLayers [8][9] provides a multi-cylinder description of the human body in order to address WBAN scenarios. It also allows to modify the radiation pattern of the antenna depending on the body antenna distance through a compact parametric model using spherical harmonics decomposition of the complex radiation pattern [10].

Within this context, this paper illustrates, through a comparison with measured data, the capability of a RT approach to recover the channel angular structure of specific Off-Body channel.

Section II provides information about the measurement setup, the chosen spatial configuration of the measured scene and the used antennas. Section III describes the modeled synthetic environment and the antennas used for simulation. Section IV focuses on the comparison between measurement and simulation in terms of path loss and angular delay spread.

II. Measurement Setup

The UWB Off-Body channel measurements have been performed at CEA-Leti in the frequency range $[3-10]$ GHz. A CTIA/IEEE standardized phantom located on a (X, Y) positioner and a 4 ports VNA have been used. The Off-Body antenna has been placed on a mast, thus representing an external access point, and three on-body antennas has been placed on the torso, the left shoulder and the back of the phantom. These on-body locations have been chosen according the application scenarios of the CORMORAN project [11].

More precisely, they represent the identified favorite on-body locations for the Coordinated Group Navigation (CGN) applications.

The measurement campaign has consisted in both obtaining received power measurements and estimating the parameters of the multi-path components (MPC) by using a SAGE algorithm [12] [13]. In particular, the estimation allows to determine the the number of paths, their amplitudes, delays and AoA. SAGE algorithm has been implemented in the frequency domain for the mathematical suitability with UWB signals.

Figures 1 illustrates the measurement setup with the Off-Body antenna and the phantom. Both are separated by a distance d_{off}. The phantom can be rotated from $0°$ to $315°$ with a step equal to $45°$. The red dots on the phantom indicate the positions of antennas. The body-worn antenna has been moved over a spatial grid, for different phantom orientation. In addition, measurements have also been realized in the absence of the human body (isolated antenna). With this setup, MPC could be determined in the case of isolated antenna and body-worn antennas. The UWB extension of the SAGE algorithm described in [14] has been employed to estimate the number of paths, their amplitudes, delays and an AoAs [15].

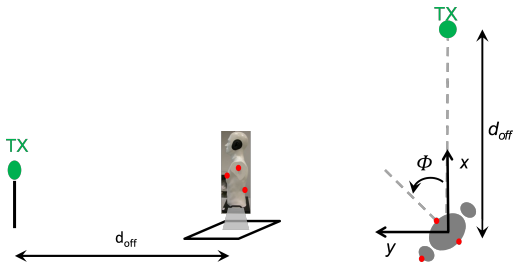

(a) (b)

Figure 1: (a) Side and (b) top representation of the Off-Body antenna and on-body antenna measurement configuration. The red dots on the phantom indicate the positions of on-body antennas on torso, shoulder and back.

A. Measurement Environment Description

Figure 2a and Figure 2b show respectively the floor plan and a picture of the measurement environment. The height between the floor and the ceil was $2.55m$ and $2.80m$ on the left half side and right half side of the room respectively. The height of the Off-Body antenna was $1.35m$ and the height of the isolated antenna was $1.33m$. Those of the antennas located on the torso, the shoulder and the back, were respectively $1.33m$, $1.40m$ and $1.35m$. Finally, the height of the phantom when placed on the positioner was $1.75m$. The green squares represent two positions of the virtual antenna array which is required for the MPC estimation of the SAGE algorithm. Let us note its size is not in scale compared to that of the room.

B. Antennas

The Off-Body antenna is an UWB Wire-patch monopole antenna, omni-directional in azimuth. Its radiation pattern in elevation for different frequency values is given in Figure 4a.

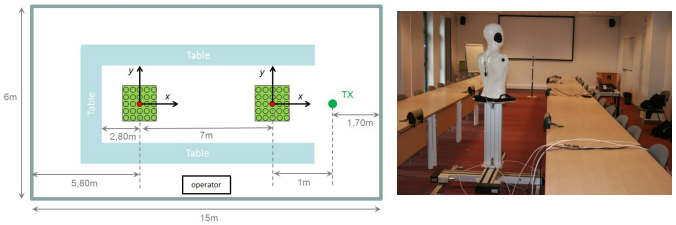

(a) (b)

Figure 2: (a) The floor map and (b) picture of the measurement environment.

The antenna placed on the body is an UWB printed dipole [16], omni-directional in azimuth in the isolated case. When the antenna is placed to the human body, its radiation pattern is modified depending on the operating frequency and distance from the body.

Furthermore, in the scenario using the isolated antenna which has been performed for studying the body influences, only one omni-directional antenna has been used at the phantom side.

III. Deterministic Simulation Setup

A. Synthetic Environment Description

The described synthetic environment is a simplify version of the layout which does not include the large table in the room. The 3 internal walls are made of $10cm$ of plaster while the outside wall is made of $7cm$ of brick. Plaster and brick properties are defined in Table I, where ϵ_r and σ are the electric permittivity and the electrical conductivity respectively.

Material	ϵ_r	σ
Plaster	8	0.038
Brick	4.9	0.3

Table I: Material properties used in RT simulation.

This environment description preserves the asymmetrical distribution of the path energy depending on the direction of arrival of the rays, because the level coming from the brick wall would be stronger than the level coming from the partition wall. In Figure 3, the rainbow colored shapes represent the antenna pattern on both transmitting and receiving sides and the black lines represent the rays obtained from a simulation. In this configuration, the two antennas are 8 meters distant. The antenna patterns correspond respectively to a wire-patch monopole (left) and to a nearby body antenna (right). The blue and red parts on the walls represent windows and the door respectively.

B. Antenna Modeling

Figure 4 shows (a) the Off-Body measured realized gain pattern of the wire-patch monopole antenna in the elevation plane, and (b) the antenna pattern used in the RT tool. The 3D simulated antenna pattern is close to measurement, with a maximum realized gain around $5dBi$ except from the

horizontal to the bottom, where the simulated antenna present a higher gain than the actual measured gain.

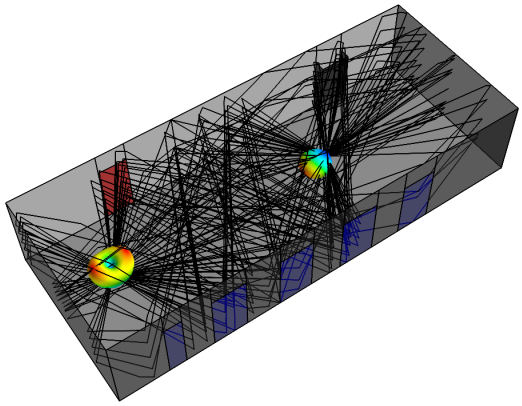

Figure 3: 3D view of the synthetic environment. The two colored shapes are the antennas radiation patterns, the blue and red parts on the walls represent the door and windows respectively, and the black lines are the the rays obtained by the RT simulation.

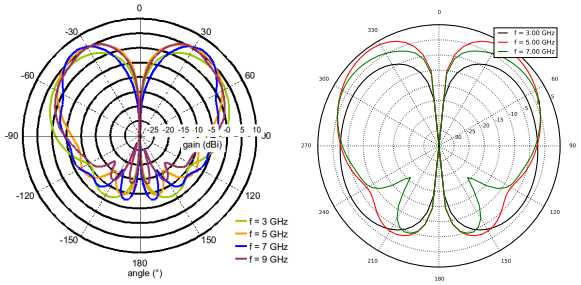

(a) Measured (b) Simulated

Figure 4: (a) Measured and (b) simulated Off-Body antenna pattern

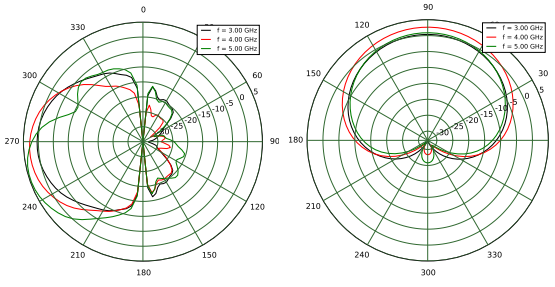

(a) Elevation (b) Azimuth

Figure 5: Body-worn antenna simulated pattern: (a) elevation and (b) azimuth

In the RT simulation, the presence of the phantom is taken into account through a perturbed antenna radiation pattern. The antenna used in measurement has been placed on cylindrical phantom with $30cm$ radius and an antenna-body separation of $5mm$. Then, the gain patterns in elevation and azimuth have been obtained from a CST MWS^{TM} simulation. These results are presented in Figure 5.

IV. Comparison Measurements vs Deterministic Simulation

In this section, the PyLayers RT simulator is used to reproduce the measurement conditions presented in the previous sections. The goal is to check the ability of the tool to provide rich channel information in a rather controlled scenario.

A. Path Loss Comparison

As a first step, it is important to check the RT tool capability to deliver consistent path loss (PL) levels regarding the antennas and the propagation environment. In particular, by using the simplified approach consisting in including the body effect only through a perturbed antenna radiation pattern.

Figure 6, Figure 7 and Figure 8 illustrate the simulated PL obtained for 3 different positions of the body mounted antenna, respectively torso, shoulder and back. Notice that, the PL is accounted unconventionally as a negative number. The simulation considers the gain patterns described in III-B, which is close to the one expected in the real channel measurements.

As expected, for both measures and simulations, the more the phantom hides the Line of Sight, the greater the absolute value of the path loss (PL). More precisely, the absolute PL value is the lowest when the phantom orientation ϕ is equal to:

- $0°$ for antenna located on the torso,
- $0°$ and/or $180°$ for antenna located on the left shoulder,
- $180°$ for antenna located on the back.

The absolute value of the PL is the highest when the phantom orientation ϕ is equal to:

- $180°$ for antenna located on the torso,
- $90°$ for antenna located on the left shoulder,
- $0°$ for antenna located on the back.

For the three scenarios, a good agreement between measurement and simulation can be observed, both quantitatively and qualitatively. The observable differences of levels are due to higher gain of the simulated Off-Body antenna in some space directions. However, it is noticeable that the simulation with realistic antennas catches the modification of the path loss exponent in situation of strong shadowing, as it was observed in measurements. Indeed at angle values of $180°$, $90°$ and $0°$ for torso, shoulder and back respectively, the dependency with distance is observed as being almost flat.

B. Angular Delay Spread Comparison

We now compare the AoA estimations obtained by the SAGE algorithm to those obtained by RT including the perturbed antennas. The simulations have been done for two distances ($d_{off} = 1m$ and $d_{off} = 8m$) in the case with no-phantom and for a single distance ($d_{off} = 8m$) in others cases. All the antenna positions on the body (Torso, Shoulder

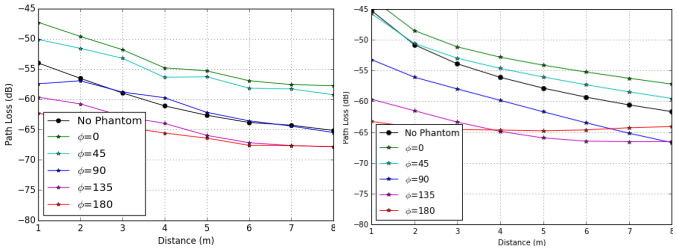

(a) Measured (b) Simulated

Figure 6: (a) Measured versus (b) Simulated Path Loss, antenna mounted on torso

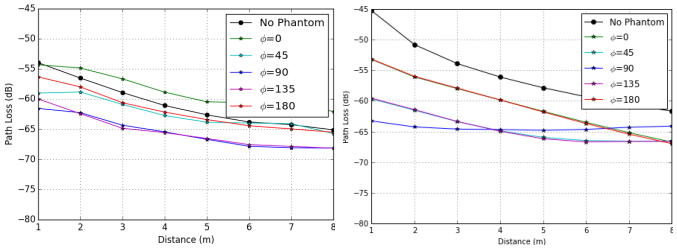

(a) Measured (b) Simulated

Figure 7: (a) Measured versus (b) Simulated Path Loss, antenna mounted on shoulder

and Back) have been evaluated. The quantity of interest is the angular delay profile. For all following figures, each MPC is represented by a point where the angle, the radius and the color represent the simulated AoA in azimuth (nearby body antenna), the propagated distance, and the MPC power respectively.

It can be noticed that, in all cases, the number of observed MPC is lower in simulation than in measurement. Specifically, simulations show that no energy is caught by the simulator between $20m$ and $40m$. This can be explained both by the lack of furnitures in the simulated environment, and by the fact that low-energy level rays are neglected. Those rays correspond to multiple bouncing rays between the walls behind the antennas. Moreover this discrepancy between simulated and measured results can depend on the SAGE algorithm tuning and capability to catch specular components.

In a first step, to have a reference situation, Figure 9 and Figure 10 compare the measurement and simulation of AoA distribution in situation without phantom, i.e. isolated antenna. This first validation step shows that both amplitude levels and angle distribution of the strongest paths are well recovered.

In the second step, we compare measurement and simulations with the body phantom. Recall that the presented simulations account for the body only through the surrounded antenna radiation pattern. For that purpose, the different antenna positions on the body have been obtained by rotating the antenna pattern.

Figure 11, Figure 12 and Figure 13 illustrate the results for the antenna placed on the torso, shoulder and back respectively, when $d_{off} = 8m$. Considering the left figure

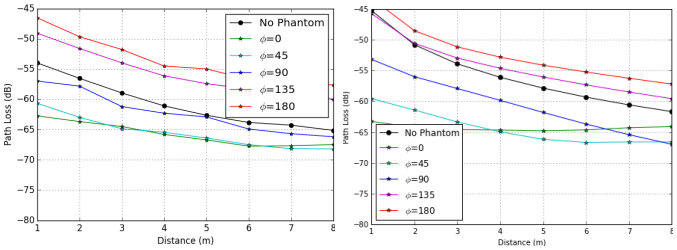

(a) Measured (b) Simulated

Figure 8: (a) Measured versus (b) Simulated Path Loss, antenna mounted on back

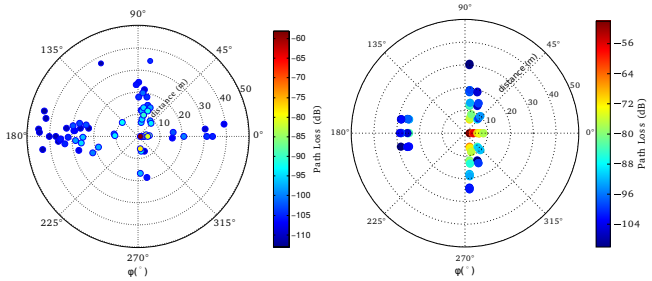

(a) Measured (b) Simulated

Figure 9: (a) Measured versus (b) Simulated AoA at 1m, isolated antenna

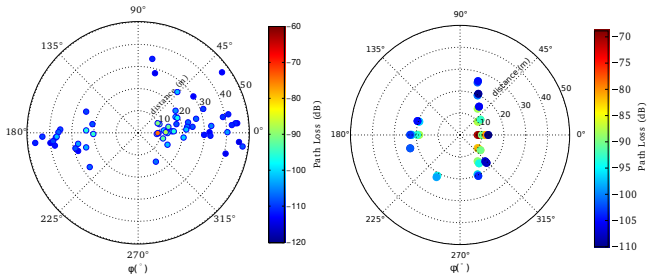

(a) Measured (b) Simulated

Figure 10: (a) Measured versus (b) Simulated AoA at 8 m, isolated antenna

corresponding to the measurement for the 3 cases, torso, shoulder and back, we can notice that the direction of arrival, $0°$, $90°$ and $180°$ receptively, are consistent with the antennas configurations. This is also true for the simulation, whereas less paths are recovered especially the weakest. It is interesting to underline that the asymmetry introduced in the layout description (brick wall on the left, plaster wall on the right when looking along x axis) is well observed in e.g. Figure 11.

For simulation, when considering the distribution of the rays in the angle/distance domain a straight vertical line is observed. This results from a geometrical fact due to the chosen RT parametrization which emphasizes the rays reflected on the lateral walls and neglects weak rays emanating from the walls behind the antennas. Then, the prevalent relation observed in simulation between distance and angle in the

azimuth plane is $d(\theta) = d_{off}/\cos(\theta)$. Adopting a richer environment and a different RT parametrization would have yielded closer simulation results.

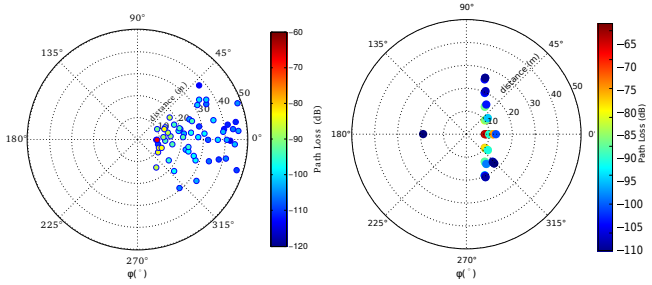

(a) Measured (b) Simulated

Figure 11: (a) Measured versus (b) Simulated AoA at 8 m, antenna mounted on torso

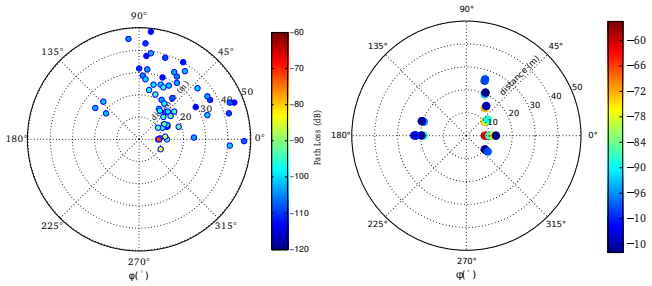

(a) Measured (b) Simulated

Figure 12: (a) Measured versus (b) Simulated AoA at 8 m, antenna mounted on shoulder

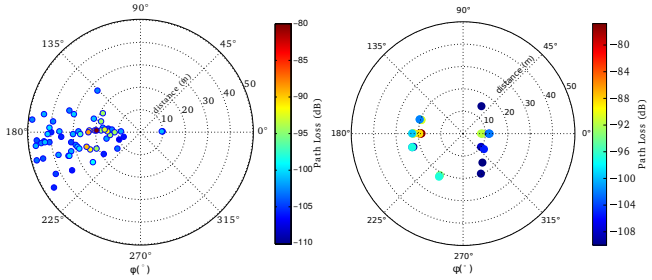

(a) Measured (b) Simulated

Figure 13: (a) Measured versus (b) Simulated AoA at 8 m, antenna mounted on back

V. Conclusion

This paper presented a comparison between data from an indoor UWB Off-Body measurement campaign on a phantom and the simulation from a site specific simulator. At that point of the investigation, the main features of the deterministic ray-tracing tool PyLayers have been validated for static scenarios starting from measurements. It has been shown that even with a simplified environment description and a fairly approximated antenna pattern on the body, the tool is able to retrieve the main channel characteristics. Moreover, it validates the idea that the influence of the human body in the channel can be modeled by a modified antenna pattern. This result open new perspectives for further PHY layer simulation, in particular for scenarios taken into consideration the body movement.

Acknowledgment

This work has been carried out in the frame of the CORMORAN project, which is funded by the French National Research Agency (ANR) under the contract number ANR-11-INFR-010.

References

[1] P. S. Hall and Y. Hao, "Antennas and propagation for body centric communications," in *Antennas and Propagation, 2006. EuCAP 2006. First European Conference on*, pp. 1–7, Nov 2006.

[2] A. Molisch, "Ultra-wide-band propagation channels," *Proceedings of the IEEE*, vol. 97, pp. 353–371, Feb 2009.

[3] R. Chavez-Santiago, K. Sayrafian-Pour, A. Khaleghi, K. Takizawa, J. Wang, I. Balasingham, and H.-B. Li, "Propagation models for ieee 802.15.6 standardization of implant communication in body area networks," *Communications Magazine, IEEE*, vol. 51, pp. 80–87, August 2013.

[4] M. Maman, B. Denis, and R. D'Errico, "Research trends in wireless body area networks: From on-body to body-to-body cooperation," in *Medical Information and Communication Technology (ISMICT), 2014 8th International Symposium on*, pp. 1–5, April 2014.

[5] G. Conway, W. Scanlon, C. Orlenius, and C. Walker, "In situ measurement of uhf wearable antenna radiation efficiency using a reverberation chamber," *Antennas and Wireless Propagation Letters, IEEE*, vol. 7, pp. 271–274, 2008.

[6] C. Roblin and A. Sibille, "Modeling of the influence of body-worn antennas upon the path loss variability in uwb wban scenarios," in *General Assembly and Scientific Symposium, 2011 URSI*, pp. 1–4, Aug 2011.

[7] S. L. Cotton, R. D'Errico, and C. Oestges, "A review of radio channel models for body centric communications," *Radio Science*, vol. 49, pp. 371–388, 2014.

[8] N. Amiot, M. Laaraiedh, and B. Uguen, "Pylayers: An open source dynamic simulator for indoor propagation and localization," in *Communications Workshops (ICC), 2013 IEEE International Conference on*, pp. 84–88, June 2013.

[9] "PyLayers." http://www.pylayers.org. Accessed: 2014-10-10.

[10] M. Mhedhbi, S. Avrillon, T. Pedersen, and B. Uguen, "Modelling of uwb antenna perturbed by human phantom in spherical harmonics space," in *Antennas and Propagation (EuCAP), 2014 8th European Conference on*, pp. 3566–3570, April 2014.

[11] "ANR CORMORAN." http://pylayers.github.io/pylayers/cormoran.html. Accessed: 2014-10-10.

[12] B. Fleury, D. Dahlhaus, R. Heddergott, and M. Tschudin, "Wideband angle of arrival estimation using the sage algorithm," in *Spread Spectrum Techniques and Applications Proceedings, 1996., IEEE 4th International Symposium on*, vol. 1, pp. 79–85 vol.1, Sep 1996.

[13] B. Fleury, M. Tschudin, R. Heddergott, D. Dahlhaus, and K. Ingeman Pedersen, "Channel parameter estimation in mobile radio environments using the sage algorithm," vol. 17, pp. 434–450, Mar 1999.

[14] Haneda, K. and Takada, J.-i., "An application of SAGE algorithm for UWB propagation channel estimation," in *Ultra Wideband Systems and Technologies, 2003 IEEE Conference on*, pp. 483–487, 2003.

[15] O. P. Pasquero and R. D'Errico, "Angle of arrival characterization in uwb indoor off-body channel," in *9th European Conference on Antennas and Propagation,*, April 2015.

[16] E. Gueguen, F. Thudor, and P. Chambelin, "A low cost uwb printed dipole antenna with high performance," in *Ultra-Wideband, 2005. ICU 2005. 2005 IEEE International Conference on*, pp. 89–92, Sept 2005.